PHILOSOPHICAL TRANSACTIONS A

royalsocietypublishing.org/journal/rsta

Research

Cite this article: Lv Z, Cheng C, Lv H. 2023 Automatic identification of pavement cracks in public roads using an optimized deep convolutional neural network model. *Phil. Trans. R. Soc. A* **381**: 20220169. https://doi.org/10.1098/rsta.2022.0169

Received: 10 July 2022
Accepted: 19 August 2022

One contribution of 15 to a theme issue 'Artificial intelligence in failure analysis of transportation infrastructure and materials'.

Subject Areas:
materials science

Keywords:
pavement distress, mask region-based convolutional neural network, transverse crack, longitudinal crack, mesh crack

Author for correspondence:
Zhihan Lv
e-mail: lvzhihan@gmail.com

Automatic identification of pavement cracks in public roads using an optimized deep convolutional neural network model

Zhihan Lv[1], Chen Cheng[2] and Haibin Lv[3]

[1]Department of Game design, Faculty of Arts, 752 36 Uppsala, Uppsala University, Sweden
[2]The Second Monitoring and Application Center, CEA, Xian, People's Republic of China
[3]North China Sea Offshore Engineering Survey Institute, Ministry Of Natural Resources North Sea Bureau, People's Republic of China

ZL, 0000-0003-2525-3074

The current study aims to improve the efficiency of automatic identification of pavement distress and improve the status quo of difficult identification and detection of pavement distress. First, the identification method of pavement distress and the types of pavement distress are analysed. Then, the design concept of deep learning in pavement distress recognition is described. Finally, the mask region-based convolutional neural network (Mask R-CNN) model is designed and applied in the recognition of road crack distress. The results show that in the evaluation of the model's comprehensive recognition performance, the highest accuracy is 99%, and the lowest accuracy is 95% after the test and evaluation of the designed model in different datasets. In the evaluation of different crack identification and detection methods, the highest accuracy of transverse crack detection is 98% and the lowest accuracy is 95%. In longitudinal crack detection, the highest accuracy is 98% and the lowest accuracy is 92%. In mesh crack detection, the highest accuracy is 98% and the lowest accuracy is 92%. This work not only provides an in-depth reference for

THE ROYAL SOCIETY PUBLISHING

the application of deep CNNs in pavement distress recognition but also promotes the improvement of road traffic conditions, thus contributing to the progression of smart cities in the future.

This article is part of the theme issue 'Artificial intelligence in failure analysis of transportation infrastructure and materials'.

1. Introduction

Since the twentieth century, especially after the Second World War, cars have become a common means of transportation for the masses, and traffic accidents have gradually become the most common personal injury accidents. At the same time, the road has suffered great damage due to long-term traffic operation, so the distress on the road surface is becoming increasingly complicated with the service time of the road [1]. The emergence of pavement distress recognition technology based on visual technology provides many intelligent recognition methods for pavement distress recognition. With strong advantages in image recognition, deep convolutional neural networks (CNNs) provide a prominent means for pavement distress recognition. Therefore, deep optimization design of pavement distress recognition technology through deep CNN is an innovative study [2].

Hameed *et al*. [3] proposed that the present pavement distress plays an important role in urban development, but the emergence of pavement distress seriously blocks the progression of urban road traffic. Therefore, comprehensive detection of roads is conducted. Identifying and resolving pavement distress is an important task in current society [3]. Han *et al*. [4] noted that pavement distress detection plays an important role in road maintenance [4]. D'Alessandro *et al*. [5] mentioned that pavement distress recognition technology needs to breakthrough manual operation and relies on scientific and technological means. It is innovative to optimize the pavement distress recognition programme by changing the application technology. Khan *et al*. [6] pointed out that to change the traditional methods of pavement distress recognition, image-based pavement distress detection has become a subject of competitive research in various countries. It takes advantage of high-speed and high-precision cameras to shoot road images quickly and uses computers for fast processing to obtain distress information [6]. Lagree *et al*. [7] proposed that in recent years, based on the continuous progression of pavement distress recognition technology, CNNs have attracted extensive attention due to their ability to automatically extract image feature expressions. Some attempts have been made to apply it to crack detection [7]. Zhou [8] pointed out that CNNs and intelligent algorithms can detect the types of pavement distress and automatically identify road conditions, helping road maintenance departments carry out daily maintenance work conveniently, efficiently and in a targeted manner [8].

In summary, first, the recognition technology of pavement distress is analysed. Then, the application of deep learning is discussed. Finally, the mask region-based convolutional neural network (Mask R-CNN) model is designed and applied to pavement distress detection. This work provides technical support for the optimization of pavement distress recognition technology and contributes to the improvement of road construction in future smart cities.

2. Pavement distress recognition and deep learning optimization

(a) Multiple distress identification on public roads

With the continuous development and progress of society, people's daily lives have been inseparable from traffic. Moreover, the speed of road surface damage has accelerated, and the detection of distress on road surfaces has become increasingly heavy [9].

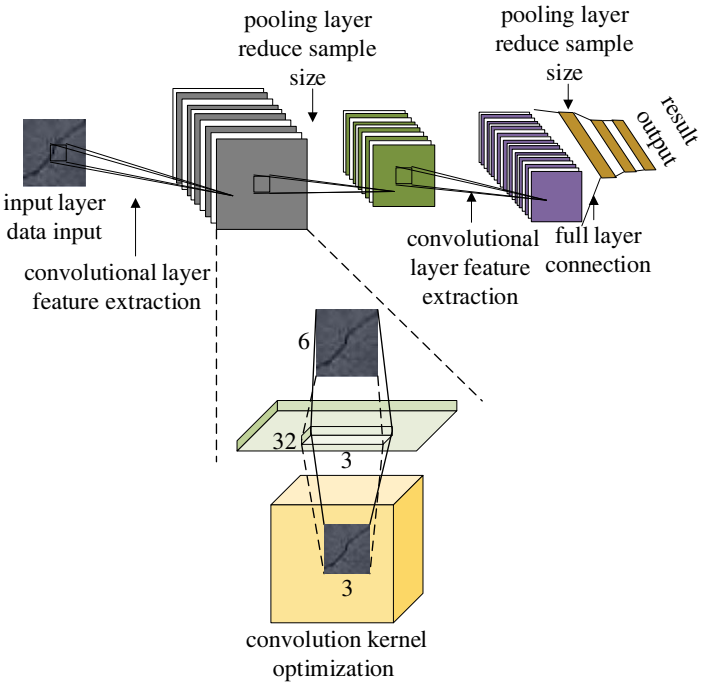

Figure 1. Model of CNN and construction of its convolutional kernel.

Among various types of urban pavement distress, crack distress is one of the most representative types of pavement distress, which is the early manifestation of other large-scale pavement distress [10]. If not repaired in time, it will develop into a more serious pavement distress type. Compared with other pavement distress types, it is more difficult to detect them [11]. In addition, pavement distress also includes potholes, ruts, looseness, subsidence and surface damage, which have a serious impact on road traffic [12]. Therefore, pavement distress is the main hazard of urban road traffic. Therefore, the accurate identification of cracks and distress on public roads through scientific and technological means plays an important role in the timely handling of distress and reducing traffic losses on public roads [13]. Common road surface distress mainly includes cracks, potholes, ruts, looseness and subsidence. The designed model carries out the comprehensive identification and detection of road pavement cracks, among which the types of cracks mainly include transverse cracks, longitudinal cracks and mesh cracks [14].

(b) Convolutional neural network-based highway distress recognition

Deep learning technology is a prominent technology in machine learning, which has important research significance in the current society. Its application fields are very wide, and its functions are also very complete, which can efficiently address various technical problems in the current society. In the field of deep learning, image recognition and feature extraction are widely studied. Deep CNN performs well in this task [15]. A deep CNN is a multi-layer alternating perceptron that can efficiently detect image features through its multi-layer comprehensive calculation and can extract image features as the technical basis of image research [16]. Figure 1 shows the CNN model and the specific structure principle of the convolutional kernel.

In figure 1, the convolution layer is the main computing layer in the CNN model, and the size and step of its convolution kernel determine its computing mode and computing capability [17]. The commonly used excitation functions are the sigmoid function and ReLU function, and their

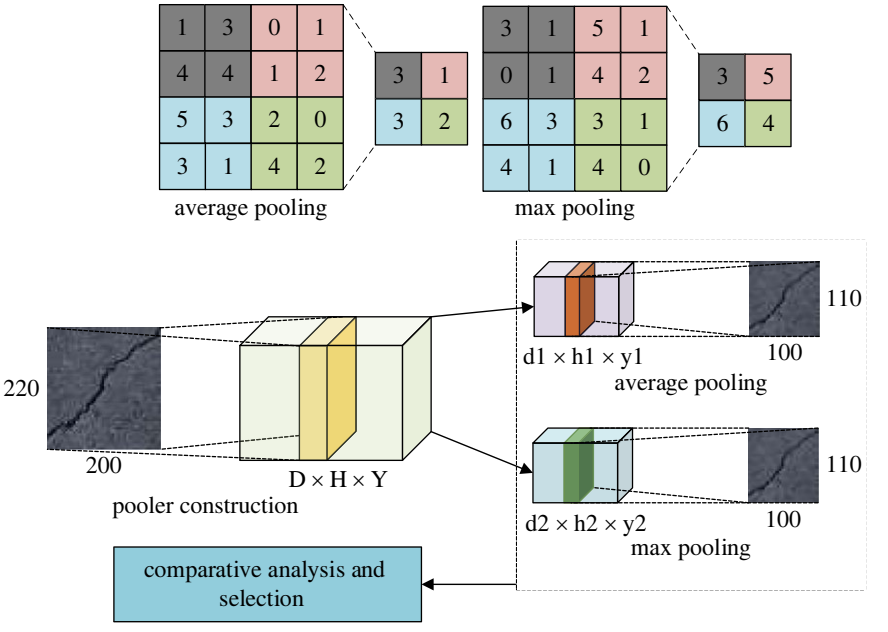

Figure 2. Two pooling operations for the pooling layer and their specific design.

calculation equations are as follows:

$$f(x) = \frac{1}{1 + e^{-x}}, \tag{2.1}$$

and

$$f(x) = \max(0, x) = \begin{cases} 0, & x < 0 \\ x, & x \geq 0 \end{cases}, \tag{2.2}$$

where x represents the calculation factor. Common pooling operations include average pooling and maximum branch pooling [18]. Figure 2 shows the two pooling operations for the pooling layer and how they work.

In figure 2, the application of the pooling layer greatly optimizes the computational efficiency of the CNN model. The fully connected layer is the terminal structure of a CNN, which is usually used to classify image features. The softmax regression classifier is commonly used, and its expression is

$$S_j = \frac{e^{z_j}}{\sum_k e^{z_k}}, \tag{2.3}$$

where k represents the number of neurons, j represents neurons and its output can be calculated as follows:

$$z_j = \sum wx + b, \tag{2.4}$$

where w represents the calculated weight, and b represents the bias of the neural network layer. The CNN model includes forward operation and reverse operation. Forward operation refers to the process of network training, which takes the calculation results of the former layer as the input of the latter layer to calculate the classification score and the probability of the current class. The reverse operation refers to reversing the output errors of the output layer to the input layer to

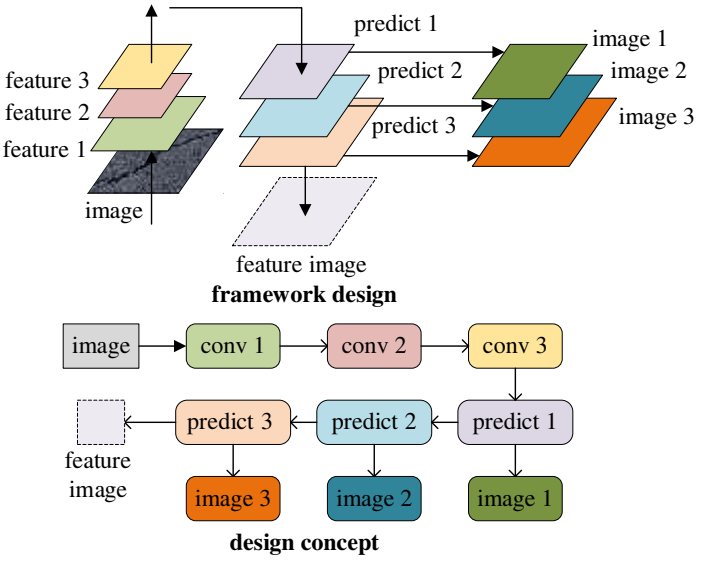

Figure 3. Optimal design of FPN.

optimize the model parameters. The error calculation formula is

$$E(W,b)=\frac{1}{2}\sum_{i=1}^{N}\| t_i-y_i\|^2, \tag{2.5}$$

where t represents the true value of the sample, i represents the serial number of the sample, y represents the predicted value of the sample and W and b represent the weight and bias of the neural network layer, respectively. The updating formula of the two is

$$W^l=W^l-\eta\frac{\partial}{\partial W^l}E(W,b), \tag{2.6}$$

and

$$b^l=b^l-\eta\frac{\partial}{\partial b^l}E(W,b), \tag{2.7}$$

where l represents the level of the neural network and η represents the learning rate of the model. Typical CNN models include the visual geometry group net model, which uses 3×3 convolutional kernels to form a deep network.

3. Design of the mask region-based convolutional neural network-based highway distress recognition model

To optimize the model, a Mask R-CNN model is designed to detect and recognize pavement distress. In the task of pavement crack identification, the detection network can be used to locate the crack, but it cannot calculate the crack length, width, area and other parameters [19]. This model using a single task (such as a detection network or segmentation network) can only complete the detection or segmentation task of road distress [20]. Moreover, the advantages of the Mask R-CNN model can be highlighted by the feature pyramid network (FPN), as illustrated in figure 3, which shows the optimization design of the model convolution process by FPN.

Figure 3 also shows the optimization design of the convolution process for the FPN network structure. Since the original Mask R-CNN algorithm uses the ResNet residual network as the skeleton network, which has good performance, is easy to train, and can be stacked with many

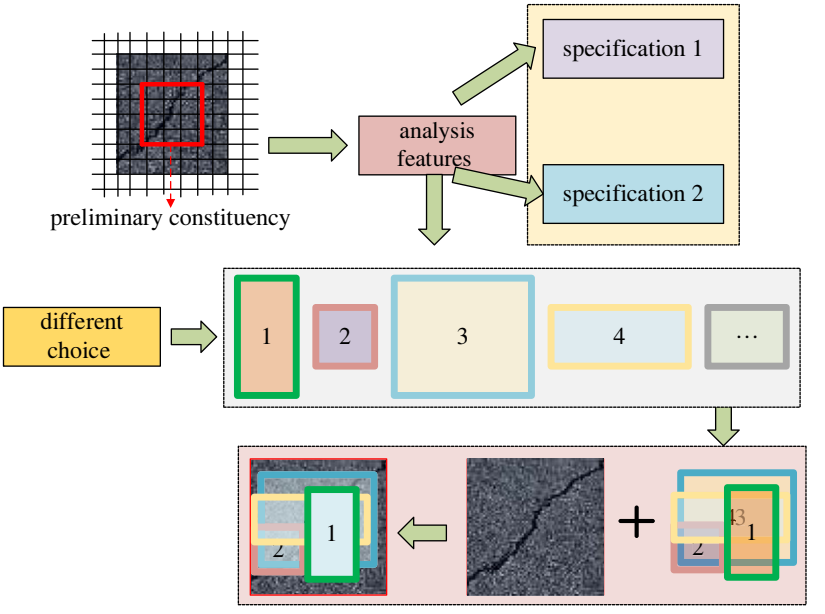

Figure 4. Optimal design of the RPN generation candidate box.

layers, ResNet is used as the basic network, and the FPN idea is added for illustration [21]. Its calculation is as follows:

$$k = k_0 + \log_2\left(\sqrt{\mathrm{wh}}/224\right), \tag{3.1}$$

where k represents the feature graph, and w and h represent the width and height of the feature graph, respectively. Then, the model's job is to generate the RPN of the candidate region, which is to generate a high-quality region candidate box. Figure 4 shows the optimized design of the RPN generation candidate box for model work.

In figure 4, the red box on the left represents a convolution kernel, and a new feature graph is generated after sliding calculation. In addition, boundary regression is used to make the positions of the candidate boxes more accurate. Usually, (x, y, w, h) is used to represent the window of candidate boxes [22]. Then, the calculation of boundary regression is as follows:

$$f(P_x, P_y, P_w, P_h) = (\hat{G}_x, \hat{G}_y, \hat{G}_w, \hat{G}_h) \approx (G_x, G_y, G_w, G_h), \tag{3.2}$$

where f represents the mapping, P represents the candidate box of prediction, G represents the box of real position and $\hat{G}$ represents the box of regression window. The principle of the equation is moving the prediction candidate box to the regression window box close to the real position through mapping. The specific calculation is as follows:

$$\Delta x = P_w d_x(P), \tag{3.3}$$

$$\Delta y = P_h d_y(P), \tag{3.4}$$

$$\hat{G}_x = P_w d_x(P) + P_x, \tag{3.5}$$

$$\hat{G}_y = P_h d_y(P) + P_y, \tag{3.6}$$

$$S_w = \exp(d_w(P)), \tag{3.7}$$

$$S_h = \exp(d_h(P)), \tag{3.8}$$

$$\hat{G}_w = P_w \exp(d_w(P)) \tag{3.9}$$

and

$$\hat{G}_h = P_h \exp(d_h(P)), \tag{3.10}$$

step 1	**start**
step 2	**Set** Configuration that will be used by the Mask-RCNN library
	class Mask R-CNN Config (mrcnn. config. Config):
	NAME = "coco_pretrained_model_config"
step 3	**for** Filter a list of Mask R-CNN detection results to get only the detected crack
	def get_car_boxes (boxes, class_ids):
	crack_boxes =[]
step 4	**for** i, box in enumerate(boxes):
	If the detected object isn't a crack, skip it
step 5	**End if**
step 6	**Until** box = $k = k_0 + \log_2(\sqrt{wh}/224))$
step 7	**Else if** $f(P_x, P_y, P_w, P_h) = (\hat{G}_x, \hat{G}_y, \hat{G}_w, \hat{G}_h) \approx (G_x, G_y, G_w, G_h)$
	$\Delta x = P_w d_x(P),\ \Delta y = P_h d_y(P), S_w = \exp(d_w(P)), S_h = \exp(d_h(P))$
step 8	**Then** $t_G = (t_x, t_y, t_w, t_h)$
step 9	**End**

Figure 5. Specific calculation flow of the Mask R-CNN model.

where Δ represents position shift and S represents scale scaling. Then, the calculation of translation and scale scaling is as follows:

$$t_x = \frac{(G_x - P_x)}{P_w}, \tag{3.11}$$

$$t_y = \frac{(G_y - P_y)}{P_h}, \tag{3.12}$$

$$t_w = \log\left(\frac{G_w}{P_w}\right), \tag{3.13}$$

$$t_h = \log\left(\frac{G_h}{P_h}\right) \tag{3.14}$$

and

$$t_G = (t_x, t_y, t_w, t_h), \tag{3.15}$$

where t_G represents the real coordinates. Figure 5 shows the specific calculation flow of the model.

In figure 5, the model predicts pavement distress through calculation and then detects and evaluates pavement distress [23]. Then, the loss function of the model can be calculated by

$$\text{Loss} = \sum_{i}^{N} (t_*^i - \widehat{w_*^T} \emptyset_5(P^i))^2 \tag{3.16}$$

and

$$W_* = \arg\min_{w*} \sum_{i}^{N} (t_*^i - \widehat{w_*^T} \emptyset_5(P^i))^2 + \lambda \parallel \hat{w}_* \parallel^2, \tag{3.17}$$

where $\emptyset_5$ represents the feature vector for the candidate area, W_* represents the learning parameter and $\widehat{w_*^T} \emptyset_5$ represents the prediction result [24]. The regression functions of the model

are as follows:

$$t_x = \frac{(x - x_a)}{w_a}, \tag{3.18}$$

$$t_y = \frac{(y - y_a)}{h_a}, \tag{3.19}$$

$$t_w = \log\left(\frac{w}{w_a}\right), \tag{3.20}$$

$$t_h = \log\left(\frac{h}{h_a}\right), \tag{3.21}$$

$$t_x^* = \frac{(x^* - x_a)}{w_a}, \tag{3.22}$$

$$t_y^* = \frac{(y^* - y_a)}{h_a}, \tag{3.23}$$

$$t_w^* = \log\left(\frac{w^*}{w_a}\right) \tag{3.24}$$

and

$$t_h^* = \log\left(\frac{h^*}{h_a}\right), \tag{3.25}$$

where a stands for the anchor point. Finally, the region of interest (ROI) align operation of the model is executed, including linear interpolation and bilinear interpolation. Its task is to accurately infer the remaining relevant data from the given data [24]. The calculation of linear interpolation is as follows:

$$y = \omega_0 y_0 + \omega_1 y_1, \tag{3.26}$$

$$\frac{y - y_0}{x - x_0} = \frac{y - y_1}{x - x_1} \tag{3.27}$$

and

$$y = \frac{x - x_0}{x_1 - x_0} y_1 + \frac{x_1 - x}{x_1 - x_0} y_0, \tag{3.28}$$

where ω represents the weight. The calculation of bilinear interpolation is as follows:

$$f(R_1) = \frac{x_2 - x}{x_2 - x_1} f(Q_{11}) + \frac{x - x_1}{x_2 - x_1} f(Q_{21}), \tag{3.29}$$

$$f(R_2) = \frac{x_2 - x}{x_2 - x_1} f(Q_{12}) + \frac{x - x_1}{x_2 - x_1} f(Q_{22}) \tag{3.30}$$

and

$$f(P) = \frac{y_2 - y}{y_2 - y_1} f(R_1) + \frac{y - y_1}{y_2 - y_1} f(R_2) \tag{3.31}$$

where R_1, R_2 and P represent two given points and a calculated point, and Q_{11}, Q_{21} and Q_{22} are transition points used in the calculation. Linear and bilinear interpolation operations are the basis of the ROI align operation [23]. The model designed in this work is aimed at the recognition of multiple road diseases, so multi-task loss is designed. The relevant loss functions include the classification loss function, regression loss function and segmentation loss function [25].

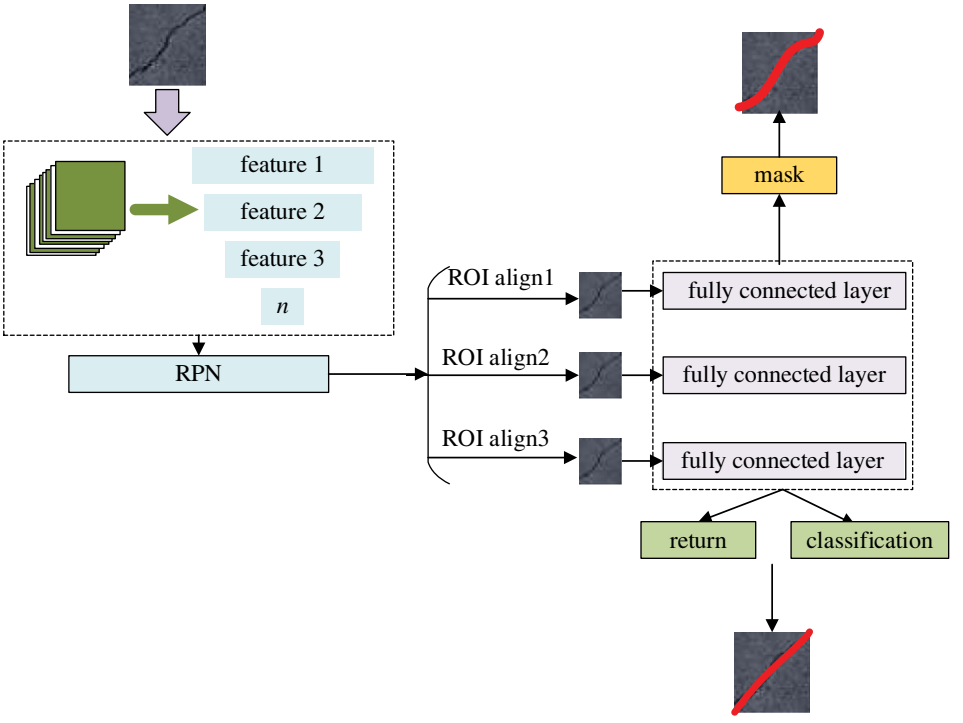

Figure 6. Comprehensive design of the Mask R-CNN model.

The designed model is for the identification of multiple distress on the road, so multi-task loss is designed. Related loss functions include the classified loss function, regression loss function and segmentation loss function [25], and their calculations are as follows:

$$L_{\text{cls}} = -\sum_{i=1}^{M} y\log(p), \tag{3.32}$$

$$L_{\text{box}} = \sum_{i\in x,y,w,h} smooth(t_i - t_i^*), \tag{3.33}$$

$$smoothL_1(x) = \begin{cases} 0.5x^2, |x| < 1 \\ |x| - 0.5, \text{others} \end{cases} \tag{3.34}$$

and

$$L_{\text{mask}} = -\frac{1}{a^2}\sum_{1\le i,j\le a} [y_{ij}\log\hat{y}_{ij}^n + (1 - y_{ij})\log(1 - \hat{y}_{ij}^n)], \tag{3.35}$$

where i and j represent pixels, y represents pixel labels, $\hat{y}_{ij}^n$ represents predicted values and n represents the hierarchy of the network. Other parameters are the same as the above equations. Figure 6 shows the comprehensive design of the optimized Mask R-CNN model.

In figure 6, the Mask R-CNN model is comprehensively optimized, thereby improving the recognition efficiency of the model for road diseases and providing technical support for the improvement of road traffic conditions [26]. The workflow of the model is first to decolour the collected image and then to extract features from the grey image. In this process, the model will also carry out convolution and pooling operations on the graph to effectively extract image features and ensure the working efficiency and final effect of the model.

Table 1. Experimental configuration.

serial number	experiment apparatus	configure
1	operating system	Windows10
2	CPU	Intel(R)_Xeon(R)_W-2133
3	memory	32G
4	graphics card	Nvidia GTX 2080Ti
5	programming language	Python3.9
6	frame type	Pytorch

4. Experimental data setting

In this work, the data used for training and evaluation of the design model are from public datasets, including the German asphalt pavement (GAP) 384 dataset [27], which contains a total of 1969 grey value images. The image resolution is 1920 × 1080 pixels, and each pixel represents 1.2 × 1.2 mm. The Cracktree 200 dataset [28] includes 206 road surface images of size 800 × 600 with various types of cracks. The Cracks and Potholes in Road Images dataset [29] is mainly a collection of defective images of paved roads in Brazil. It contains 2235 images from highways, including roads, cracks and potholes. The structural defects network (SDNET) 2018 dataset [30] contains more than 56 000 images of cracked and non-cracked concrete bridge decks, walls and walkways. The dataset includes cracks as narrow as 0.06 mm and as wide as 25 mm. The dataset also includes images with various obstacles, including shadows, surface roughness, scaling, edges, holes and background debris. In the identification of road defects, the model designed in this work includes lateral cracks, longitudinal cracks and mesh cracks. The main method aims to preliminarily identify and detect the length of various cracks through the input test model of the images in the dataset, of which a total of 500 images are detected in this work. In table 1, the basic information of the computer hardware devices for simulation detection in this work is displayed.

5. Evaluation of convolutional neural network-based pavement distress recognition model

(a) Comparative evaluation of optimization performance of convolutional neural network model

By designing and optimizing the Mask R-CNN model, highway distress recognition technology is realized to comprehensively improve the model's recognition and detection effect and improve the current highway distress detection status. Figure 7 shows the evaluation results of the crack detection accuracy of the model.

In the detection of pavement distress cracks, the model is tested and evaluated in four datasets, and it is found that the detection accuracy of the model is 99% at the highest and 95% at the lowest (figure 7). Figure 8 shows the evaluation results of the designed model for the identification of different cracks.

In figure 8, DLA refers to detecting lateral cracks, DLO refers to detecting longitudinal cracks, DM refers to detecting mesh cracks, CLA refers to cutting lateral cracks, CLO refers to cutting longitudinal cracks and CM refers to cutting mesh cracks. The results show that the highest accuracy of the model is 98% and the lowest accuracy is 87% in transverse crack detection.

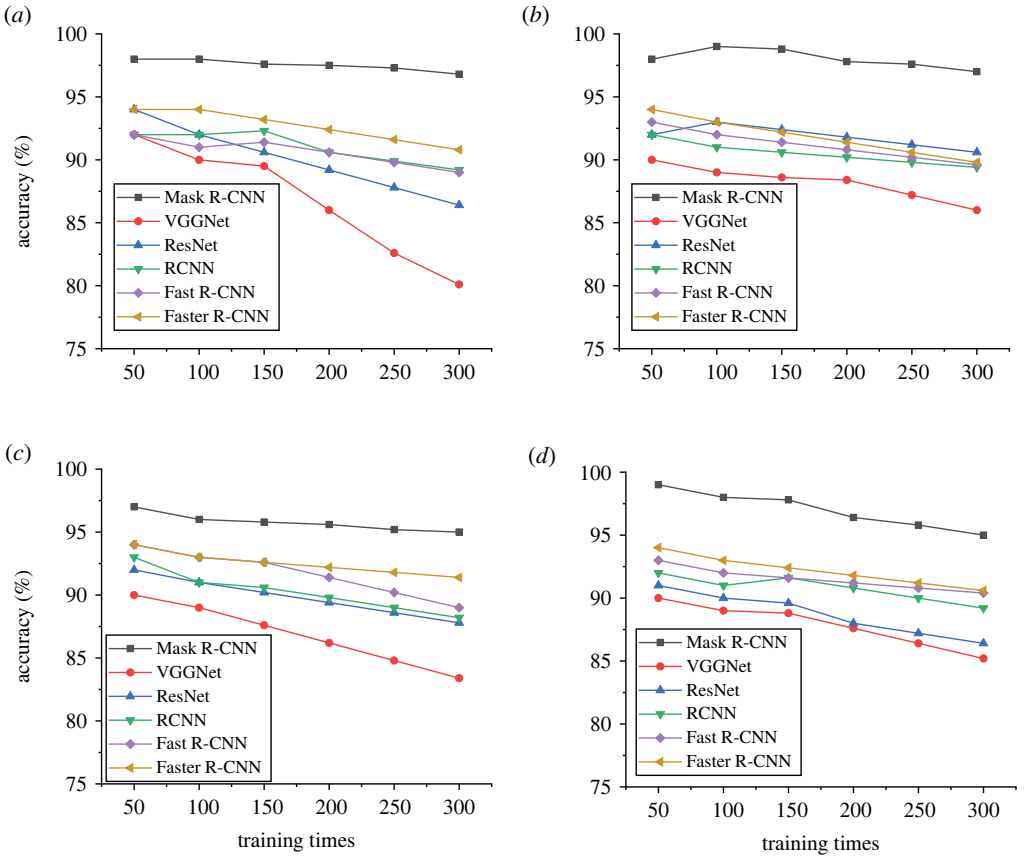

Figure 7. Evaluation of pavement distress detection accuracy ((*a*) the GAP dataset, (*b*) the Cracktree 200 dataset, (*c*) the CPRI dataset and (*d*) the SDNET dataset).

(b) Mask region-based convolutional neural network model detection performance evaluation

The optimized model can calculate the specific length of cracks by predicting the movement distance of the frame. Therefore, this model is a breakthrough of traditional crack identification technology to a certain extent and provides a more advantageous model for the identification of cracks. Figure 9 shows the evaluation results of the test time for different crack lengths.

In figure 9, the legend represents the detection times. The results show that the longest detection time of the model is 32 ms, the lowest is 25 ms, the longest cutting time of the model is 48 ms and the lowest is 30 ms. In addition, the length detection and cutting accuracy of the model are very high. Figure 10 shows the evaluation results of the length detection accuracy of the model.

In figure 10, in the detection of pavement cracks, the model has a very high detection accuracy of length, with the highest detection accuracy 98% and the lowest detection accuracy 90%. In the cutting process, the accuracy of the model is 98% and 92%, respectively. Figure 11 shows the loss value evaluation results of this model in road surface distress detection.

In figure 11, the loss value of the model in the detection is very low. In crack identification, when the number of loss iterations of the model is 7, the loss value is close to the minimum value and the minimum loss value of the model is maintained at 0.25. In crack length detection, the loss value of the model is slightly higher, but when the number of zone times of the model is 10 times, it is close to the lowest and tends to be stable, while the loss value of the model is 0.5.

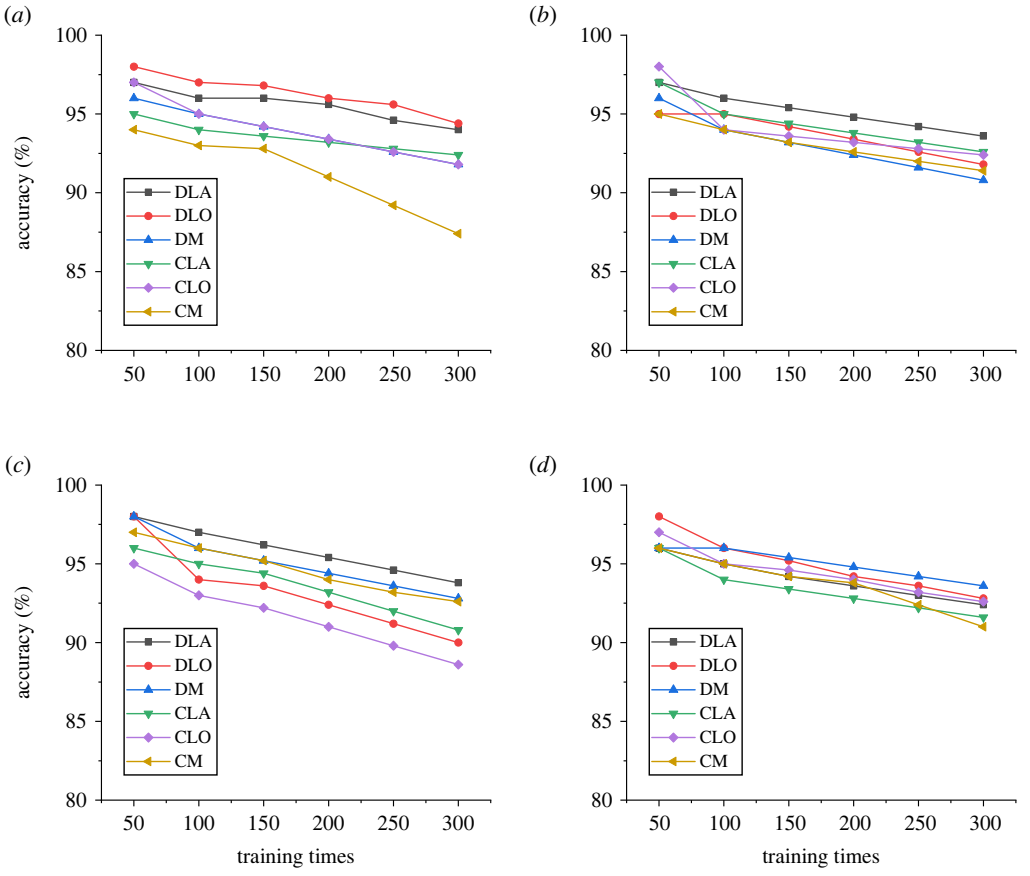

Figure 8. Identification and evaluation of different cracks by the Mask R-CNN model ((*a*) the GAP dataset, (*b*) the Cracktree 200 dataset, (*c*) the CPRI dataset and (*d*) the SDNET dataset).

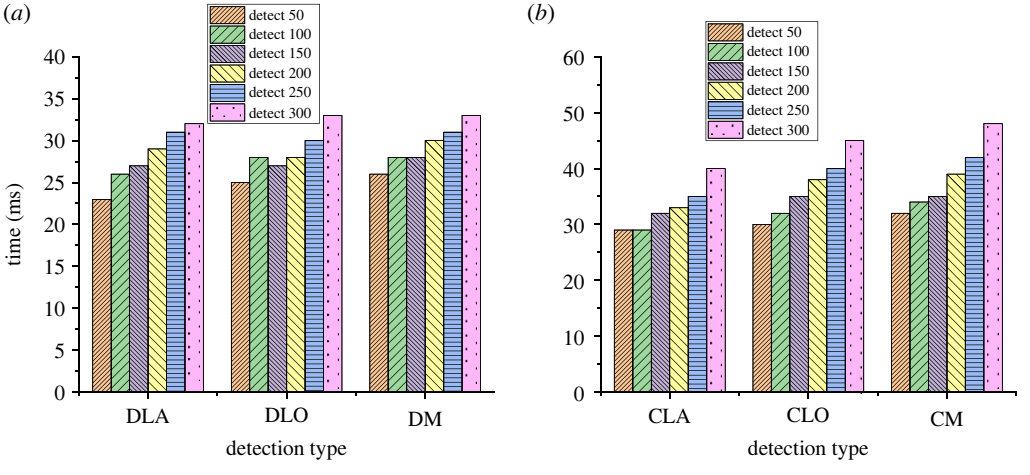

Figure 9. Evaluation of detection time for different crack lengths ((*a*) detection, (*b*) cutting).

6. Conclusion

With the development of the economy, road traffic has been affected by many kinds of transportation tools, so the road is inevitably damaged. Based on this, the recognition technology

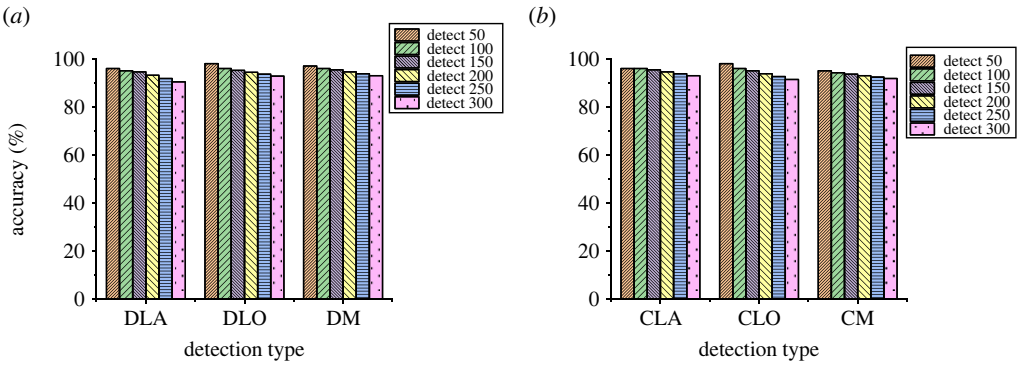

Figure 10. Evaluation of the length detection accuracy of the model ((*a*) detection, (*b*) cutting).

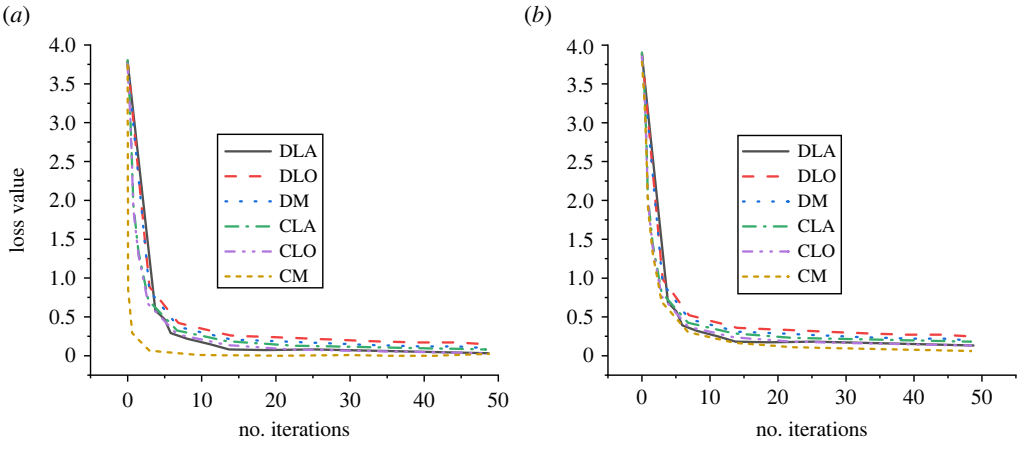

Figure 11. Loss values in pavement distress detection ((*a*) the loss of crack recognition, (*b*) the loss of crack length detection).

of road surface diseases and the types of road diseases are discussed. Then, the application design of deep learning technology in road disease recognition is introduced. Finally, based on deep CNN technology, the Mask R-CNN model is designed for the recognition of road crack disease, and the designed model is comprehensively evaluated and detected. The results show that in the evaluation of model comprehensive recognition performance, the designed model is tested and evaluated in different datasets, and the detection accuracy of the model is the highest, which is superior to other recognition techniques in all aspects. Second, the accuracy of the designed model is always higher than 92% in transverse fracture detection, longitudinal fracture detection and mesh fracture detection. The accuracy of transverse cracks, longitudinal cracks and mesh cracks is always higher than 87%. In the crack length detection, the longest detection time of the model is approximately 32 ms, and the shortest detection time is approximately 25 ms. The longest cutting time of the model is approximately 48 ms, and the shortest is approximately 30 ms. In the detection accuracy, the highest is approximately 98% and the lowest is approximately 90%. In cutting, the highest accuracy of the model is approximately 98% and the lowest is approximately 92%. Finally, the loss value of this model in detection is very low. In fracture identification, when the number of loss iterations of the model is approximately 7, the loss value is close to the minimum value of approximately 0.25. In fracture length detection, the loss value of the model is slightly higher, but the model is close to the lowest loss value of approximately 0.5 when the number of iterations is approximately 10. Although a better model is designed and

comprehensive evaluation results are provided in this work, the application effect of the model in the actual environment is not tested in the model evaluation. At the same time, the evaluation factors used are not comprehensive enough, so more comprehensive reference factors will be designed in future research to further evaluate the performance of the model and design a more comprehensive model application concept.

Data accessibility. The raw data supporting the conclusions of this article are available upon request.

Authors' contributions. Z.L.: investigation, validation, writing—original draft and writing—review and editing; C.C.: data curation, validation and writing—original draft; H.L.: investigation, supervision, validation and writing—original draft.

All authors gave final approval for publication and agreed to be held accountable for the work performed therein.

Conflict of interest declaration. The authors have no conflict of interest.

Funding. We received no funding for this study.

References

1. Zhang X *et al.* 2021 A deep learning integrated radiomics model for identification of coronavirus disease 2019 using computed tomography. *Sci. Rep.* **11**, 1–12. (doi:10.1038/s41598-020-79139-8)
2. Capra M, Bussolino B, Marchisio A, Shafique M, Masera G, Martina M. 2020 An updated survey of efficient hardware architectures for accelerating deep convolutional neural networks. *Fut. Internet* **12**, 113. (doi:10.3390/fi12070113)
3. Hameed BZ, S. Dhavileswarapu AV, Naik N, Karimi H, Hegde P, Rai BP, Somani BK. 2021 Big data Analytics in urology: the story so far and the road ahead. *Ther. Adv. Urol.* **13**, 1756287221998134. (doi:10.1177/1756287221998134)
4. Han J, Gatheral T, Williams C. 2020 Procalcitonin for patient stratification and identification of bacterial co-infection in COVID-19. *Clin. Med. Res.* **20**, e47–e47. (doi:10.7861/clinmed.Let.20.3.3)
5. D'Alessandro F, Di Mascio P, Lombardi L, Ridolfi B. 2022 Methodology for the identification of economic, environmental and health criteria for road noise mitigation. *Noise Mapping* **9**, 10–22. (doi:10.1515/noise-2022-0002)
6. Khan A, Sohail A, Zahoora U, Qureshi AS. 2020 A survey of the recent architectures of deep convolutional neural networks. *Artif. Intell. Rev.* **53**, 5455–5516. (doi:10.1007/s10462-020-09825-6)
7. Lagree A, Mohebpour M, Meti N, Saednia K, Lu FI, Slodkowska E, Tran WT. 2021 A review and comparison of breast tumor cell nuclei segmentation performances using deep convolutional neural networks. *Sci. Rep.* **11**, 1–11. (doi:10.1038/s41598-021-87496-1)
8. Zhou DX. 2020 Universality of deep convolutional neural networks. *Appl. Comput. Harmon. A* **48**, 787–794. (doi:10.1016/j.acha.2019.06.004)
9. Lacoursiere RE, Hadi D, Shaw GS. 2022 Acetylation, phosphorylation, ubiquitination (Oh My!): following post-translational modifications on the ubiquitin road. *Biomolecules* **12**, 467. (doi:10.3390/biom12030467)
10. Silva-Spínola A, Baldeiras I, Arrais JP, Santana I. 2022 The road to personalized medicine in Alzheimer's disease: the use of artificial intelligence. *Biomedicines* **10**, 315. (doi:10.3390/biomedicines10020315)
11. Worachairungreung M, Ninsawat S, Witayangkurn A, Dailey MN. 2021 Identification of road traffic injury risk prone area using environmental factors by machine learning classification in Nonthaburi, Thailand. *Sustainability* **13**, 3907. (doi:10.3390/su13073907)
12. Yu Z et al. 2021 Air pollution, surrounding green, road proximity and Parkinson's disease: a prospective cohort study. *Environ. Res.* **197**, 111170. (doi:10.1016/j.envres.2021.111170)
13. Grijota-Martínez C, Bárez-López S, Gómez-Andrés D, Guadaño-Ferraz A. 2020 MCT8 deficiency: the road to therapies for a rare disease. *Front. Neurosci.* **14**, 380. (doi:10.3389/fnins.2020.00380)
14. Petersen ML, Bresolin M, Monteiro AM. 2021 521-The link between olfactory dysfunction and dementia: the road so far. *Int. Psychogeriatr.* **33**(S1), 69–70. (doi:10.1017/S1041610221002167)

15. Abbas A, Abdelsamea MM, Gaber MM. 2021 Classification of COVID-19 in chest X-ray images using DeTraC deep convolutional neural network. *Appl. Intell.* **51**, 854–864. (doi:10.1007/s10489-020-01829-7)
16. Narin A, Kaya C, Pamuk Z. 2021 Automatic detection of coronavirus disease (covid-19) using X-ray images and deep convolutional neural networks. *Pattern Anal. Appl.* **24**, 1207–1220. (doi:10.1007/s10044-021-00984-y)
17. Tang YX *et al.* 2020 Automated abnormality classification of chest radiographs using deep convolutional neural networks. *NPJ* **3**, 1–8. (doi:10.1038/s41746-020-0273-z)
18. Wang L, Lin ZQ, Wong A. 2020 Covid-net: a tailored deep convolutional neural network design for detection of covid-19 cases from chest x-ray images. *Sci. Rep.* **10**, 1–12. (doi:10.1038/s41598-019-56847-4)
19. Kherraki A, El Ouazzani R. 2022 Deep convolutional neural networks architecture for an efficient emergency vehicle classification in real-time traffic monitoring. *Int. J. Artif. Intell.* **11**, 110. (doi:10.11591/ijai.v11.i1.pp110-120)
20. Bhujel A, Kim NE, Arulmozhi E, Basak JK, Kim HT. 2022 A lightweight attention-based convolutional neural networks for tomato leaf disease classification. *Agriculture* **12**, 228. (doi:10.3390/agriculture12020228)
21. Taha MF *et al.* 2022 Using deep convolutional neural network for image-based diagnosis of nutrient deficiencies in plants grown in aquaponics. *Chemosensors* **10**, 45. (doi:10.3390/chemosensors10020045)
22. Goenka N, Tiwari S. 2022 AlzVNet: a volumetric convolutional neural network for multiclass classification of Alzheimer's disease through multiple neuroimaging computational approaches. *Biomed. Signal. Process.* **74**, 103500. (doi:10.1016/j.bspc.2022.103500)
23. Mahmood T, Li J, Pei Y, Akhtar F, Rehman MU, Wasti SH. 2022 Breast lesions classifications of mammographic images using a deep convolutional neural network-based approach. *PLoS ONE* **17**, e0263126. (doi:10.1371/journal.pone.0263126)
24. Cengil E, Çınar A. 2022 Hybrid convolutional neural network based classification of bacterial, viral, and fungal diseases on tomato leaf images. *Concurr. Comput.* **34**, e6617. (doi:10.1002/cpe.6617)
25. Kaur P, Harnal S, Tiwari R, Upadhyay S, Bhatia S, Mashat A, Alabdali AM. 2022 Recognition of leaf disease using hybrid convolutional neural network by applying feature reduction. *Sensors* **22**, 575. (doi:10.3390/s22020575)
26. Sboev A, Sboeva S, Moloshnikov I, Gryaznov A, Rybka R, Naumov A, Selivanov A, Rylkov G, Ilyin V. 2022 Analysis of the full-size Russian corpus of internet drug reviews with complex NER labeling using deep learning neural networks and language models. *Appl. Sci.* **12**, 491. (doi:10.3390/app12010491)
27. Papanikolaou G, Centi G, Perathoner S, Lanzafame P. 2022 Catalysis for e-Chemistry: need and gaps for a future de-fossilized chemical production, with focus on the role of complex (direct) syntheses by electrocatalysis. *ACS Cataly.* **12**, 2861–2876. (doi:10.1021/acscatal.2c00099)
28. Sholevar N, Golroo A, Esfahani SR. 2022 Machine learning techniques for pavement condition evaluation. *Autom. Constr.* **136**, 104190. (doi:10.1016/j.autcon.2022.104190)
29. Srivastava GK, Vemavarapu MM. 2021 Drillability prediction in some metamorphic rocks using composite penetration rate index (CPRI)–An approach. *Int. J. Min. Sci. Technol.* **31**, 631–641. (doi:10.1016/j.ijmst.2021.05.010)
30. Lac L, Keresztes B, Louargant M, Donias M, Da Costa JP. 2022 An annotated image dataset of vegetable crops at an early stage of growth for proximal sensing applications. *Data Brief* **42**, 108035. (doi:10.1016/j.dib.2022.108035)